NeuroImage: Clinical 9 (2015) 592–598

Contents lists available at ScienceDirect

NeuroImage: Clinical

journal homepage: www.elsevier.com/locate/ynicl

Comparison of qualitative and quantitative imaging characteristics of [^{11}C]PiB and [^{18}F]flutemetamol in normal control and Alzheimer's subjects

James M. Mountz[a,*], Charles M. Laymon[a], Ann D. Cohen[b], Zheng Zhang[c], Julie C. Price[a], Sanaa Boudhar[d], Eric McDade[e], Howard J. Aizenstein[b], William E. Klunk[b,e], Chester A. Mathis[a]

[a]Department of Radiology, University of Pittsburgh, Pittsburgh, PA, USA
[b]Department of Psychiatry, University of Pittsburgh, Pittsburgh, PA, USA
[c]Department of Biostatistics, Brown University, Providence, RI, USA
[d]Biostatistician-Pennsylvania trials, American College of Radiology, Philadelphia, PA, USA
[e]Department of Neurology, University of Pittsburgh, Pittsburgh, PA, USA

ARTICLE INFO

Article history:
Received 29 April 2015
Received in revised form 14 September 2015
Accepted 9 October 2015
Available online 14 October 2015

Keywords:
[^{11}C]Pittsburgh Compound B
[^{18}F]Flutemetamol
Alzheimer's disease
Positron Emission Tomography

ABSTRACT

Introduction: Neuritic amyloid plaques and neurofibrillary tangles, the hallmark pathologic lesions of Alzheimer's disease, are thought to develop before the symptoms of brain failure are clinically detectable. Imaging methods capable of detecting the presence of neuritic amyloid plaques should improve a clinician's ability to identify Alzheimer's disease during the earliest symptomatic phase and to identify at-risk individuals presymptomatically. Currently the best studied amyloid imaging ligand is [^{11}C]Pittsburgh Compound B ([^{11}C]PiB). However, the 20-minute half-life of this radiotracer limits its use. This study is designed to evaluate the performance characteristics of [^{18}F]flutemetamol and to independently compare results to [^{11}C]PiB in the same subjects.
Methods: Twenty-three subjects, 15 cognitively normal (NL) and 8 with a clinical diagnosis of Alzheimer's Dementia (AD), underwent [^{11}C]PiB and [^{18}F]flutemetamol PET scans within 28 days of study enrollment. We studied both normal and AD subjects to assess the uptake characteristics across a range of amyloid positivity. Blinded visual reads were conducted by five raters. Correlation analyses were performed between cortical SUVR for the two tracers and also between rater scores and SUVR for each tracer. Overall reader accuracy for classifying scans as amyloid positive or negative was determined for each tracer using SUVR classification as the standard.
Results: The linear correlation coefficient between global cortical SUVR for the two tracers was $R^2 = 0.85$, indicating that both tracers have similar retention characteristics. The two tracers were well correlated for rater-determined AD-like positivity (Cohen $\kappa = 0.82$). Averaged visual ratings and global cortical SUVR disagreed on their classification in 2/23 [^{11}C]PiB scans and 4/23 [^{18}F]flutemetamol scans.
Conclusions: [^{11}C]PiB and [^{18}F]flutemetamol have similar retention characteristics across a range of amyloid negative to positive subjects. Both tracers performed similarly when a standardized visual read technique was used to classify scans as amyloid-positive or amyloid-negative and correlated well with SUVR classifications. However, care in visual interpretation of amyloid positive versus amyloid negative regions should be taken, particularly in the case of [^{18}F]flutemetamol when considering cortical vs. white-matter retention.

1. Introduction

Alzheimer's dementia (AD) is the most common form of dementia in the elderly, affecting more than 4 million people in the United States. Although the etiology of AD has not been definitively established, converging evidence suggests that the Aβ peptide may play an important role in the pathogenesis of the disease. Accumulation of Aβ fibrils in the form of amyloid plaques is one of the hallmarks of the disease and is a key component of the neuropathological criteria for autopsy-based confirmation of diagnosis (Hyman and Trojanowski, 1997; Mirra et al., 1991).

Imaging techniques utilizing radiolabeled positron emission tomography (PET) tracers that bind to the aggregated Aβ peptides in amyloid plaques have the potential to directly assess relative brain amyloid plaque pathology. The importance of PET with Pittsburgh Compound-B, N-methyl-[^{11}C]2-(4′-methylaminophenyl)-6-hydroxybenzothiazole (also known as [^{11}C]PiB) as a research tool is well established. Nevertheless, the short half-life (20 min) of the ^{11}C radiolabel limits its utility as a tool for community-based diagnostic screening and therapeutic

* Corresponding author at: Division of Nuclear Medicine, Department of Radiology, University of Pittsburgh Medical Center, 200 Lothrop Street, Pittsburgh, PA 15213, USA.
E-mail address: mountzjm@upmc.edu (J.M. Mountz).

http://dx.doi.org/10.1016/j.nicl.2015.10.007

evaluation. This shortcoming could be addressed by the development of an ^{18}F-labeled tracer with kinetics similar to those of [^{11}C]PiB. The radiological half-life (109 min) of such a tracer would allow its distribution from centralized production facilities as in the case of ^{18}F-labeled fluorodeoxyglucose (FDG), which is now in widespread use in community-based clinics.

The present study is designed to compare the imaging characteristics of a novel ^{18}F-labeled amyloid ligand, [^{18}F]flutemetamol, to those of [^{11}C]PiB in the same subjects, across a range of brain amyloid accumulation. The performance of a visual read technique for both tracers was also evaluated by comparison to quantitative measures. A brief background of these two tracers is provided below.

The PET radiotracer [^{11}C]PiB has been developed for in vivo imaging of amyloid plaque (Klunk et al., 2004; Mathis et al., 2003). Studies have shown that [^{11}C]PiB retention in AD subjects is substantially higher than that of controls in specific cortical areas subject to AD-related Aβ accumulation but is similar in areas without Aβ deposition (e.g., subcortical white matter, cerebellum). Subjects with a diagnosis of mild cognitive impairment (MCI) exhibit [^{11}C]PiB retention spanning both the control and AD retention levels (Engler et al., 2004, 2006; Head et al., 2012; Kemppainen et al., 2007; Klunk et al., 2004; Pike et al., 2007a; Rowe et al., 2007).

A recently developed ^{18}F-labeled amyloid binding radiotracer structurally related to [^{11}C]PiB that has been proposed as an amyloid imaging agent is [^{18}F]flutemetamol. A phase 2 study has shown (Vandenberghe et al., 2010) that [^{18}F]flutemetamol selectively labels Aβ plaques in a manner similar to [^{11}C]PiB.

2. Materials and methods

2.1. Subjects

Subjects from the University of Pittsburgh Alzheimer's Disease Center longitudinal study cohort between 55 and 90 years of age were eligible for this study. All participants signed University of Pittsburgh IRB approved informed consent. Clinical cognitive assessment, including standardized measures of cognition, behavior, and function, described by National Alzheimer's Coordinating Center (NACC) Uniform Data Set, version 2.0, served as the basis for study enrollment and cohort assignment.

Testing and clinical dementia rating assessment was completed within three months prior to enrollment. Eligibility requirements for enrollment in the normal (NL) cohort included: Mini Mental State (MMS) score between 27 and 30; clinical dementia rating (CDR) score of 0; and cognitive impairment scores of no less than 1 standard deviation below the established age- and education-adjusted means for the ADC–NACC Uniform Cognitive Assessment Battery. Eligibility requirements for enrollment in the probable AD (AD) cohort included: MMS scores between 16 and 27; CDR score ≥0.5; and probable Alzheimer's disease based on NINCDS–ADRDA criteria.

At the time of subject enrollment, demographic information was recorded and a complete medical history and physical examination was performed. Patients with contraindications for MRI, e.g., those with aneurysm clips or metal fragments in the body were excluded. Subjects with significant neurologic disease, such as cerebral infarctions, history of significant head trauma or MRI brain scans showing evidence of clinically meaningful abnormalities as well as subjects with psychiatric disorders including serious major depression, history of schizophrenia, or history of substance abuse (DSM-IV criteria) were also excluded. A total of 8 patients with a clinical diagnosis of probable Alzheimer's disease and 15 cognitively normal elderly subjects were recruited into the study from March 10, 2009 to September 30, 2010. Participants in the normal cohort had mean age 71 years (range 59 to 84), whereas the Alzheimer's cohort had mean age 75 years (range 57 to 87). Participants in the normal cohort had mean MMS score 29 (range 27 to 30), compared with the Alzheimer's cohort, with mean score 21 (range 16 to 27). Subject demographics are listed in Table 1.

Table 1
Study subject demographics.

	Normal	Alzheimer's
Number of subjects	15	8
Age (years)		
Mean (SD)	71 (8.49)	75 (10)
Median	68	75
Min	59	57
Max	84	87
Gender, n (%)		
Male	5 (33)	4 (50)
Female	10 (67)	4 (50)
Race, n (%)		
Black or African American	1 (7)	1 (12.5)
White	14 (93)	7 (87.5)
MMSE Score		
Mean (SD)	29 (0.91)	21 (4.37)
Median	30	21
Min	27	16
Max	30	27
Global CDR, n (%)		
0.0—No impairment	14 (93.3)	0
0.5—Questionable impairment	1 (6.7)	2 (25)
1.0—Mild-impairment	0	5 (62.5)
2.0—Moderate impairment	0	1 (12.5)
3.0—Severe impairment	0	0

As stated in the Introduction, the goal of this study is to compare imaging characteristics of two amyloid tracers. It is not aimed at evaluating tracer efficacy for identifying patients with clinically diagnosable AD. For the purpose of achieving our goal, it was desirable that our subjects exhibit a range of amyloid load. To help achieve this, a subset ($n = 6$) of NL subjects were selected to participate in this study based on the results of a prior positive PiB scan.

2.2. Radiotracer production

The full radiosyntheses of [^{11}C]PiB (Wilson et al., 2004) and [^{18}F]flutemetamol (Mason et al., 2009) are described elsewhere.

2.3. Imaging protocol

The Alzheimer's Disease Neuro-Initiative (ADNI) MRI protocol (3D rapid gradient echo (MP-RAGE) and an axial proton density scan) was performed prior to the PET imaging procedure (Jack et al., 2008). If an ADNI MRI had been performed within the 6 months prior to enrollment, it was not repeated. Each participant underwent two PET scanning sessions, one using the [^{11}C]PiB tracer and another using [^{18}F]flutemetamol. Both PET scans were completed within 29 days of subject enrollment.

Due to the relatively short half-life of ^{11}C, in cases where the ^{11}C tracer was injected first, it was possible for subjects to receive both scans on the same day. In such cases (7 of 8 AD and 11 of 15 NL) a minimum elapsed time of 2 h (six ^{11}C half-lives) was required between [^{11}C]PiB and [^{18}F]flutemetamol injections.

The remaining 5 subjects had the two scans on different days. One NL subject had the [^{18}F]flutemetamol scan 28 days before the [^{11}C]PIB scan. The other 3 NL and 1 AD subject had their [^{11}C]PIB scans first (scan separation of 7, 6, and 7 days for NL and 29 days for AD).

Under the [^{11}C]PiB protocol, subjects were injected with 15 ± 1.5 mCi of tracer administered over a 20-second period. PET scanning commenced 50 min after injection and data were acquired for 20 min in 4 frames, each of 5 min duration (i.e., 50–70 min post-injection scan).

Under the [^{18}F]flutemetamol protocol, subjects were injected with 10 mCi of tracer and scanning commenced 90 min after injection. Data were acquired for 30 min using six 5-minute frames (i.e., 90–120 min

post-injection scan). In each case, prior to the emission scan, 10 min of transmission data, required for attenuation and scatter correction, were acquired. All PET data were acquired on a Siemens/CTI ECAT HR+ BGO scanner operating in 3-D mode (axial field-of-view: 15.5 cm; 63 planes).

2.4. Image processing

Acquired PET data were reconstructed into a 128 × 128 × 63 (axial) matrix with voxel dimensions of 0.21 × 0.21 × 0.24 cm. Reconstruction was performed using manufacturer supplied software and included corrections for attenuation, scatter, random coincidences and dead time. Images for regional analysis were processed using Fourier rebinning (FORE) followed by direct Fourier reconstruction. Images were smoothed with a 3 mm Hann filter. Following reconstruction, image sets were inspected and, if necessary, corrected for inter-frame motion. Each subject's [^{11}C]PiB and [^{18}F]flutemetamol scans were separately registered to the subject's AC–PC oriented MR scan using an Automated Image Registration (AIR) technique (Woods et al., 1993). A summation over the time frames was performed to produce a single time-frame image, i.e., a 50–70 min [^{11}C]PiB image and a 90–120 min [^{18}F]flutemetamol image for each subject.

Images for the visual reads were produced by first summing the sinograms over the time frames, followed by FORE rebinning and then reconstruction using OSEM with 4 iterations of 16 subsets. Although subject MR scans were not used for the visual reads, the PET scans were registered to MR scans as described above for the purpose of bringing them into uniform AC–PC alignment. No smoothing was applied to these images, however, in each case a new image was formed by summing adjacent axial planes resulting in a final axial plane thickness of 0.48 cm (2 × 0.24 cm).

2.5. Data analysis

2.5.1. Identification of brain regions for analysis

Five cortical brain sub-regions known to accumulate amyloid plaques in AD were selected for tracer retention analysis: anterior cingulate; precuneus; frontal cortex; parietal cortex; and lateral temporal cortex.

To investigate potential differences in nonspecific retention between [^{11}C]PiB and [^{18}F]flutemetamol the pons region was also analyzed. The pons is generally spared from amyloid plaque accumulation and this white-matter rich area has substantial nonspecific signal (Price et al., 2005).

Region-of-interest (ROI) boundaries were manually-defined using the structural MRI for anatomical reference and criteria that have proven to provide highly reproducible outcomes (Rosario et al., 2011). The Rosario et al. publication also shows examples of regional delineations on MRI scan section (as shown in Fig. 1).

2.5.2. Regional analysis

A normalized regional analysis was performed in which the cerebellar cortex was designated as the reference region for nondisplaceable (i.e., free and nonspecific) retention. Mean concentrations for the regions described above were obtained for all subjects and both tracers. Normalized regional retention values (SUVR) were produced by dividing each regional concentration by the concentration within the cerebellum ROI from the same image. An overall global cortical SUVR value was determined by averaging the SUVR values from the 5 cortical subregions.

2.5.3. Visual analysis

A standard visual analysis procedure, outlined in the following subsections, was established at a reader protocol/training meeting at the University of Pittsburgh. The protocol was developed using a set of [^{11}C]PIB and [^{18}F]flutemetamol images from amyloid-positive and amyloid-negative subjects. Otherwise, the training scans were not included in the study reported herein.

2.5.3.1. Overview. Study scans were independently evaluated by five raters (JMM, WEK, ADC, EM, HJA; all experienced neuroimaging researchers). Raters were blinded to subject identity and diagnosis; separate identifiers were used for the [^{11}C]PIB and [^{18}F]flutemetamol studies, preventing cross identification of scans. Raters first evaluated the PiB scans followed by Flutemetamol scans. At any given time, scans from only the tracer under evaluation were available to readers, i.e. during [^{11}C]PIB evaluation, [^{18}F]flutemetamol scans were inaccessible and vice versa.

Following initial read completion, the five raters met as a group for a consensus read. Two separate sessions were held; one for [^{11}C]PIB and one for [^{18}F]flutemetamol. In any case with less than 100% agreement in the individual ratings, the scans were projected for simultaneous viewing, and an attempt was made to arrive at a consensus opinion. The predetermined consensus rules were that if at least four of the raters agreed after the discussion, a consensus rating was generated, otherwise, the case would be scored “no consensus.” We note here that a consensus was arrived at in all cases.

2.5.3.2. Image presentation. Before commencement of the visual reads, the readers agreed that images would initially be displayed using a continuous colormap, without visual breaks. Thus images were displayed using a reader adjustable Hot Metal color scheme with the scale initially spanning the full image intensity range.

While the reader was free to view any slice or to use an orthogonal viewing tool, the following minimal procedure was used. All slices were first simultaneously observed on a single display page for evidence of obvious positive signal. Following this, the following axial slices were examined in an enlarged, single slice format: (1) a slice at the first appearance of lateral ventricles (going from superior to inferior) and (2) every axial slice until the cerebellar peduncles were reached. Seven consecutive sagittal slices centered at the midline were also reviewed.

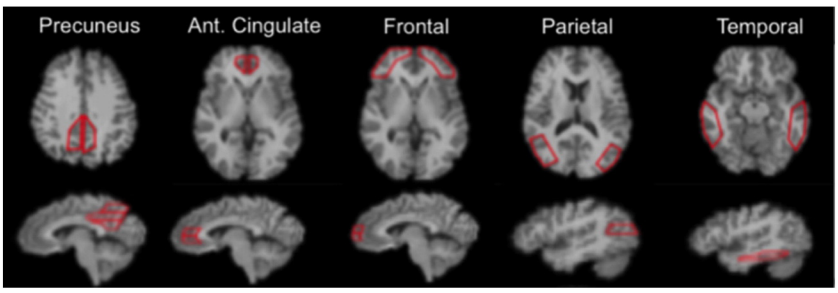

Fig. 1. Image example of the ROIs provided to visual raters. The 5 brain regions (10 total ROI) indicated are those generally attributed to be the typical AD pattern, which is generally considered as a bilaterally symmetric pattern of positivity in the frontal, parietal and temporal cortices, anterior cingulate and precuneus.

2.5.3.3. Visual scan rating. Readers were asked to provide scores for the following 3 evaluations in the order specified. In these descriptions, "positivity" is defined to be gray matter signal greater than or equal to signal in white matter regions such as pons, cerebellar peduncles, and subcortical white matter. Except for the guidance material provided for evaluation #3, described below, the visual ratings were performed using the PET scans only, i.e., without reference to subjects' MRI or other anatomical images. Visual classification examples are shown in Fig. 2.

1) Any-Region Positivity: a statement of certainty as to whether the scan was amyloid-positive in any gray matter area. This reading was not limited to the five gray matter areas listed below. Score definitions were: 1 = definitely negative; 2 = probably negative; 3 = probably positive; 4 = definitely positive.
2) AD-like Positivity: a statement of certainty as to whether the typical AD regional pattern was present (same numerical ratings as above). The typical AD pattern was considered a generally bilaterally symmetric pattern of positivity in the frontal, parietal and temporal cortices, anterior cingulate and precuneus. Cases were allowed to be frontally predominant or posteriorly predominant, but cases that were only positive in focal areas (e.g., unilateral occipital pole) were to be rated "2 = probably negative" from this "AD-like" perspective. Readers were instructed that this AD-like score could be lower than the "Any-Region" score, but could never be higher.
3) Individual Region Positivity: because visual reads were to be correlated to the normalized regional retention values, scans were visually evaluated with reference to the same ROIs as were used for the quantitative analyses. To this end, readers were provided with a hard copy depiction of orthogonal views of example ROIs overlaid on a typical MRI (Fig. 1). Each of the 10 individual regions (frontal, parietal, temporal cortices, anterior cingulate and precuneus; right and left separately) were scored (rater regional score) using the same 1–4 scale described above. A five-region average score (rater regional average) was calculated as the simple arithmetic mean of the 10 unilateral ROI scores and was correlated to the global cortical SUVR.

2.5.4. Statistical analyses

In parts of this and the following sections, threshold values for global cortical SUVR are used to classify scans as amyloid positive or negative, i.e. PiB(+), PiB(−). For [^{11}C]PiB, the threshold (1.51) was established in a separate study (Cohen et al., 2013) using an objective sparse K-means (SKM) with tight clustering approach. For the purposes of the current study, the corresponding [^{18}F]flutemetamol threshold (1.66) was obtained by transforming the PiB threshold using the global cortical SUVR correlation parameters determined in the "Correlation of [11C]PiB and [18 F]flutemetamol SUVR within Subjects" analysis described below (Section 3.1.1).

2.5.4.1. Correlation of [11C]PiB and [18 F]flutemetamol SUVR within subjects. Spearman's correlation coefficients (r) were used to determine the correlation between the [^{18}F]flutemetamol and [^{11}C]PiB SUVR values for each of the five cortical sub-regions as well as for the global cortical retention value (i.e., the 5-subregion average) within subjects. Similar correlation coefficients were also calculated for pons SUVR.

2.5.4.2. Agreement between raters and tracers. Agreement between all 5 raters was determined by Fleiss' kappa (Fleiss, 1971) and was also expressed as overall agreement as well as agreement across all cases (Cicchetti and Feinstein, 1990; Spitzer and Fleiss, 1974).

Agreement between the two tracers for rater evaluation of any-region positivity (concensus) and separately for AD-like positivity was quantified using Cohen's kappa (Cohen, 1960).

2.5.4.3. Correlation of rater regional average to global SUVR. Global cortical (5-subregion average) SUVR was compared to the rater regional-average averaged across raters (i.e. rater regional scores, ranging from 1 to 4, averaged across 10 regions and 5 raters). Results are expressed both graphically and numerically (by Spearman's correlation coefficient, r), for each tracer separately.

2.5.4.4. Correlation of rater regional score to regional SUVR. SUVR values for each of the 10 cortical regions were compared to the averaged (across raters) rater regional scores of each of the 10 regions described above for both of the tracers. Results were expressed in terms of linear correlation coefficients.

2.5.4.5. Agreement between visual classification and quantitative based classification of amyloid-positivity. An overall comparison of visual finding of amyloid positivity versus SUVR classification of amyloid positivity

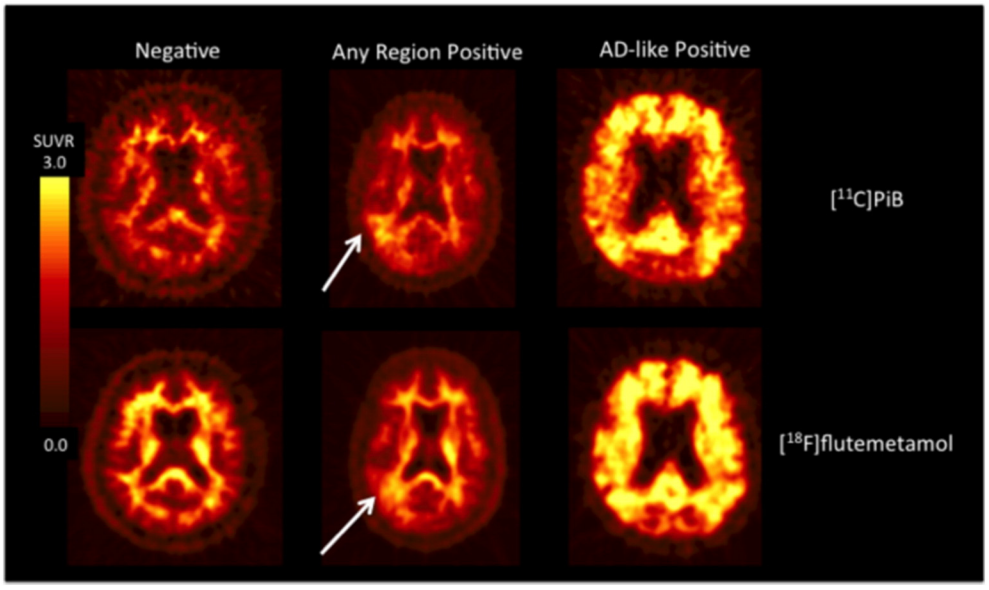

Fig. 2. Examples of [^{11}C]PiB and [^{18}F] flutemetamol scans. The top row shows [^{11}C]PiB images that are classified as (left-to-right) "Negative", "Any-region positive", and "AD-like positive." The bottom row shows these classifications for [^{18}F]flutemetamol. The arrows indicate the basis for the "Any-region positive" positivity (in this case, right posterior temporoparietal) classifications.

was performed. Images for which the consensus rating for AD-like positivity was 3 or greater were classified as amyloid positive by visual read, otherwise images were classified as amyloid negative by visual read. The global SUVR thresholds described in Section 2.5.4 were used to further classify each image as amyloid positive or negative by SUVR. For each tracer separately, agreement between visual and SUVR classification was expressed in terms of Cohen's kappa and percent agreement.

The SUVR threshold for amyloid positivity was 1.51 for [^{12}C]PiB and 1.66 for [^{18}F]flutemetamol (see Section 2.5.4).

3. Results

3.1. Correlation of [^{11}C]PiB and [^{18}F]flutemetamol SUVR within subjects

SUVR between the two tracers were compared as described in Section 2.5.4.1. Results for cortical regions are reported in the subsection 3.1.1. Sub-section 3.1.2 describes the results for the pons and cerebellum.

3.1.1. Cortical regions

Table 2 compares the uptake distribution, as measured by regional SUVR, of [^{18}F]flutemetamol and [^{11}C]PiB retention within the same subjects for both NL and AD subjects. The Spearman's correlation coefficients were high between [^{18}F]flutemetamol and [^{11}C]PiB SUVR levels for all five cortical sub-regions (0.89 or higher) as well as globally. Fig. 3 shows [^{18}F]flutemetamol versus [^{11}C]PiB global cortical SUVR for all subjects. A high degree of linear correlation between the two tracers was found; linear regression ($y = 0.80\times + 0.45$, $R^2 = 0.85$) indicated that both tracers have similar retention characteristics. The slope of 0.8 indicates that the dynamic range for [^{18}F]flutemetamol is lower that [^{11}C]PiB. The lower SUVR range of [^{18}F]flutemetamol resulted from the combination of both higher global region cortical SUV in the amyloid-positive [^{11}C]PIB subjects relative to that for [^{18}F]flutemetamol (n = 12: [^{18}F]flutemetamol, 1.00 ± 0.24; [^{11}C]PIB, 1.17 ± 0.36; P = 0.003 paired *t*-test, P = 0.219 Wilcoxon signed-rank test) and the slightly lower cortical gray matter global region SUV in the amyloid-negative [^{11}C]PIB subjects relative to that for [^{18}F]flutemetamol.

3.1.2. Pons and cerebellum

The pons SUVR showed no difference between normal elderly and AD subjects for either tracer (P = 0.96 for [^{18}F]flutemetamol and P = 0.73 for [^{11}C]PiB, both by *t*-test). However, the pons SUVR was greater for [^{18}F]flutemetamol, relative to [^{11}C]PiB for both NL and AD subjects (P < 0.0001 by paired *t*-test).

Related to its use as a potential reference region, the average [^{18}F]flutemetamol SUV in pons for all subjects in this study was significantly higher than for [^{11}C]PiB (n = 23: [^{18}F]flutemetamol = 1.44 ± 0.32; [^{11}C]PiB = 1.16 ± 0.22; P < 0.0001 paired *t*-test, P = 0.003 Wilcoxon signed-rank test).

This was not the case for the cerebellar cortex reference region where the average [^{18}F]flutemetamol SUV was slightly less than that for [^{11}C]PiB (n = 23: [^{18}F]flutemetamol = 0.53 ± 0.11; [^{11}C]PiB = 0.59 ± 0.10; P = 0.002 paired *t*-test, P = 0.055 Wilcoxon signed-rank test).

Table 2
Spearman's correlation coefficients for [^{18}F]flutemetamol and [^{11}C]PiB SUVR levels for all five cortical sub-regions.

Cortical region	Spearman's correlation
Anterior cingulate	0.92 (<0.0001)
Posterior cingulate/precuneus	0.89 (<0.0001)
Frontal cortex	0.89 (<0.0001)
Parietal cortex	0.89 (<0.0001)
Lateral temporal cortex	0.89 (<0.0001)
Global cortical region	0.90 (<0.0001)
Pons	0.61 (<0.001)

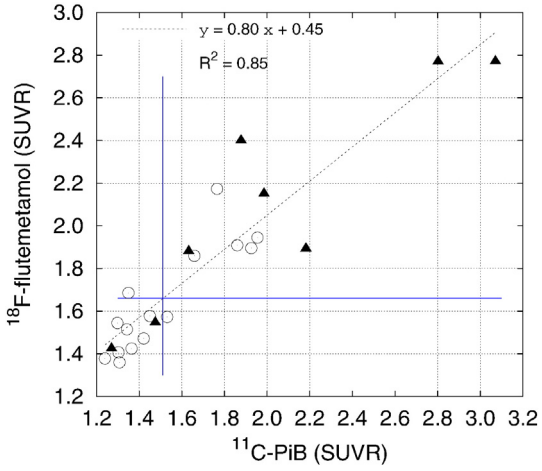

Fig. 3. Plot of the [^{18}F]flutemetamol global SUVR versus [^{11}C]PiB global SUVR values for NL and AD subjects (N = 23). Triangles indicate AD subjects and circles indicate NL subjects. Blue lines indicate the positivity thresholds for [^{11}C]PiB (vertical) and [^{18}F]flutemetemol. The six circles to the right of the vertical blue line are the PiB positive NL subjects.

3.2. Agreement between raters and tracers

Agreement between the raters was determined as described in Section 2.5.4.2. Among the 5 raters, there was (91.3%) agreement for AD-like-positive [^{11}C]PiB scans (Fleiss κ = 0.83) and there was (85.8%) agreement for any-region positive [^{11}C]PiB scans (Fleiss κ = 0.73). In the case of [^{18}F]flutemetamol scans, there was (91.3%) agreement for AD-like-positive (Fleiss κ = 0.83) and (81.7%) agreement for any-region positive scans (Fleiss κ = 0.63).

Using the consensus rating for the 5 raters for both AD-like and any-region positivity, there was agreement between the two tracers in (91.7%, Cohen κ = 0.82) cases for AD-like positivity and in (83.3%, Cohen κ = 0.67) cases for any-region positivity.

3.3. Correlation of rater regional average to global SUVR

Rater regional averages were compared to global SUVR as explained in Section 2.5.4.3. For [^{11}C]PiB, the correlation coefficient between Global cortical SUVR and the averaged visual ratings was highly significant [Fig. 4, ($R^2 = 0.63$, P < 0.0001)]. Averaged visual ratings and global cortical SUVR disagreed on their classification of two scans, where the scans were rated as PiB positive quantitatively by global cortical SUVR but PiB negative by averaged visual classification.

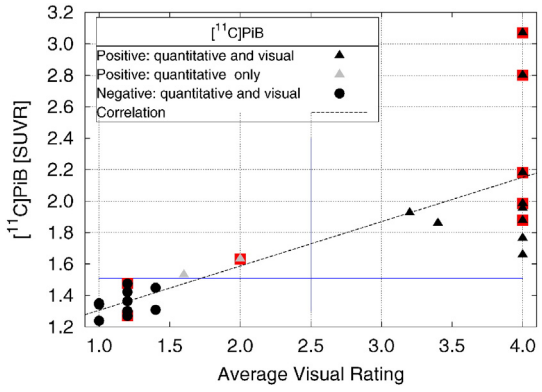

Fig. 4. Plot of [^{11}C]PiB SUVR vs. visual rating for all subjects. Black triangles indicate a PiB(+) rating by both SUVR and visual ratings, black circles indicate a PiB(−) rating by both SUVR and visual ratings. Gray triangles indicate a PiB(+) rating by SUVR and a PiB(−) visual rating. Points for subjects with a clinical AD diagnosis are under-struck with a red box. The line is the result of a linear regression over all 23 subjects ($y = 0.28\times + 1.02$; $R^2 = 0.63$).

The correlation coefficient between Flutemetamol global cortical SUVR and the averaged visual ratings was highly significant [Fig. 5, ($R^2 = 0.72$, $P < 0.0001$)]. Visual ratings and SUVR disagreed on their classification of four scans, where the scans were rated as positive quantitatively by global cortical SUVR but negative by averaged visual classification.

3.4. Correlation of rater regional score to regional SUVR

Regional SUVR and rater regional scores were correlated as described in Section 2.5.4.4. Correlation coefficients (R^2) ranged between 0.44–0.70 for [^{11}C]PiB and 0.65–0.78 for [^{18}F]flutemetamol (Table 3).

3.5. Agreement between visual classification and quantitative based classification of amyloid-positivity

Classification of amyloid positivity by visual read and by SUVR is described in Section 2.5.4.5. For [^{11}C]PiB classifications disagreed in 2/23 cases (91.3% agreement) with Cohen's kappa = 0.833. For [^{18}F]flutemetamol classifications disagreed in 4/23 cases, (82.6% agreement) with a Cohen's kappa = 0.652.

4. Discussion

Both [^{11}C]PiB and [^{18}F]flutemetamol have been shown to robustly and reliably label brain amyloid plaques (Curtis et al., 2015; Engler et al., 2004, 2006; Kemppainen et al., 2007; Klunk et al., 2004; Pike et al., 2007a; Rowe et al., 2007; Wolk et al., 2011). The goal of this study was to compare the two tracers in the same AD and NC subjects using both visual reads and SUVR to evaluate amyloid positivity and correlate [^{11}C]PiB and [^{18}F]flutemetamol.

In our study sample, 6 of the15 NL subjects had evidence of amyloid deposition. It is important to note that in this study, these 6 subjects were specifically chosen based on their prior PiB(+) status to assess the uptake characteristics across a range of amyloid positivity. Therefore, the proportion of PiB(+) NL subjects in this study (40%) is higher than some previous reports (Aizenstein et al., 2008; Apostolova et al., 2010; Furst et al., 2010; Mormino et al., 2009; Pike et al., 2007b; Rentz et al., 2010; Resnick et al., 2010).

Good correlation was observed between [^{11}C]PiB and [^{18}F]flutemetamol in SUVR of individual cortical regions and in global cortical average SUVR (Fig. 3, Table 2). Additionally, we found that there was also good agreement between the two tracers in classifying subjects as amyloid-positive.

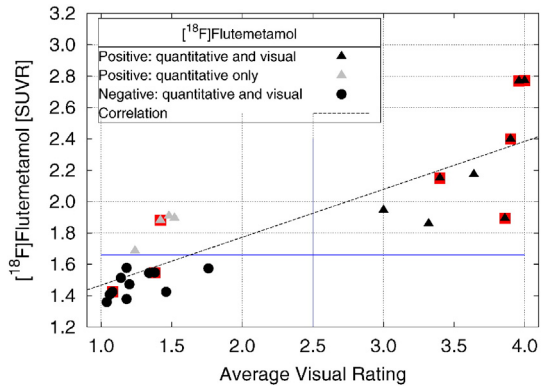

Fig. 5. Plot of [^{18}F]flutemetamol vs. visual rating for all subjects. Black triangles indicate a Flute(+) rating by both SUVR and visual ratings, black circles indicate a Flute(−) rating by both SUVR and visual ratings, and gray triangles indicate a Flute(+) rating by SUVR and a Flute(−) visual rating. Points for subjects with a clinical AD diagnosis are under-struck with a red box. The line is the result of a linear regression over all 23 subjects ($y = 0.31x + 1.16$; $R^2 = 0.72$).

Table 3
Correlation coefficients (R^2) of rater regional score to regional SUVR for the Left (L) and Right (R) posterior cingulate/precuneus (PX), anterior cingulate (AC), frontal cortex (FR), parietal cortex (PR), lateral temporal cortex (LT).

	RPX	LPX	RAC	LAC	RFR	LFR	RPR	LPR	RLT	LLT
PiB	0.669	0.652	0.696	0.676	0.642	0.614	0.444	0.498	0.530	0.511
Flute	0.783	0.705	0.660	0.720	0.736	0.721	0.691	0.658	0.704	0.652

However, there were some differences of note between the two radiotracers. As evidenced by the slope of the correlation line in Fig. 3, the SUVR dynamic range of [^{18}F]flutemetamol is smaller than that of [^{11}C]PIB. This is not attributable to the denominator of the (SUVR) ratio, as the average cerebellar cortex reference region value for [^{18}F]flutemetamol was lower than that for [^{11}C]PiB. Instead, the lower SUVR range of [^{18}F]flutemetamol likely results from the combination of both higher global region cortical SUV signal in the amyloid-positive [^{11}C]PIB subjects relative to that for [^{18}F]flutemetamol and the slightly lower cortical gray matter global region SUV in the amyloid-negative [^{11}C]PIB subjects relative to that for [^{18}F]flutemetamol as described above (i.e., a larger range in the numerator of the ratio for [^{11}C]PIB).

When examining the agreement across visual raters for both [^{11}C]PiB and [^{18}F]flutemetamol there was overall good agreement in rating subjects as AD-like amyloid-positive (Section 3.2). There was, however, a tendency to assign visual ratings of any-region amyloid positive to [^{18}F]flutemetamol scans that were, objectively (by SUVR SKM classification, translated from PiB), amyloid negative. This is thought to reflect the inclination to rate higher white matter retention (see Fig. 2) as cortical [^{18}F]flutemetamol retention. The clinical significance of these differences is likely to be more of a concern for individuals with low levels of amyloid deposition or no amyloid deposition than for those who are clearly positive (i.e. AD-like). This highlights the critical need for careful training in the visual rating of any amyloid imaging ligand that exhibits appreciable white matter retention.

There was also a significant correlation between visual rating and the SUVR for both [^{11}C]PiB and [^{18}F]flutemetamol. As Fig. 4 depicts, there was disagreement between the visual classification [PiB(−)] and the objective SUVR classification [PiB(+)] in only two subjects. The agreement between SUVR classification and visual ratings for amyloid positivity with [^{18}F]flutemetamol was slightly less than that of [^{11}C]PiB with disagreement between the classification for 4 subjects (all objective amyloid-positive and visual amyloid-negative Fig. 5). In addition, it is interesting to note that for the most part, when a scan was PiB(+) via SUVR SKM rating, raters tended to have high confidence (a visual rating score of 4) that the scan was indeed PiB(+); however, the raters had slightly less confidence with the visual rating for [^{18}F]flutemetamol (i.e. more visual rating scores between 3 and 4), likely a result of higher white matter retention in the [^{18}F]flutemetamol images (see Figs. 2, 4 and 5).

The correlations of individual cortical SUVR values to the visual rating of these individual cortical regions also yielded quite interesting results. While the correlations between all cortical SUVR values to the visual rating scores were significant for both tracers, the most significant correlations were in anterior cingulate and precuneus, which is noteworthy for two reasons. First, amyloid deposition in both anterior cingulate and precuneus are very typically observed in AD and an SKM analysis with regional weighting identified anterior cingulate and precuneus as the two regions with the highest weights, meaning that these regions were most relevant to the analyses. Second, the fact that both anterior cingulate and precuneus are midline gray matter regions in which essentially two thicknesses of cortex are adjacent to each other without intervening white matter may accentuate the appearance of specific tracer retention in these areas, particularly in the case of [^{18}F]flutemetamol.

5. Conclusion

There is a high degree of linear correlation between [^{18}F]flutemetamol and [^{11}C]PiB across all brain regions indicating that both tracers have similar retention characteristics. Both tracers performed similarly when a standardized visual read technique was used to classify scans as amyloid-positive or amyloid-negative and visual reads correlated well with SUVR classifications. However, care in interpretation of amyloid positive versus amyloid negative regions must be taken, particularly in the case of [^{18}F]flutemetamol, when considering cortical vs. white-matter retention.

Acknowledgments

This project is funded, in part, under a grant (ACRIN-PA 4004) with the Pennsylvania Department of Health to the American College of Radiology Imaging Network (ACRIN). The Department specifically declaims responsibility for any analyses, interpretations or conclusions. Additional support, in part, from grants NIH P50 AG005133, P01 AG025204 and R37 AG025516 is acknowledged. We also greatly appreciate the recruitment efforts of Ms. Claire McConaha.

References

Aizenstein, H.J., Nebes, R.D., Saxton, J.A., Price, J.C., Mathis, C.A., Tsopelas, N.D., Ziolko, S.K., Snitz, B.E., Houck, P.R., Bi, W., Cohen, A.D., Lopresti, B.J., DeKosky, S.T., Halligan, E.M., Klunk, W.E., 2008. Amyloid deposition is frequent and often is not associated with significant cognitive impairment in the elderly. Arch. Neurol. 65 (11), 1509–1517.

Apostolova, L.G., Hwang, K.S., Andrawis, J.P., Green, A.E., Babakchanian, S., Morra, J.H., Cummings, J.L., Toga, A.W., Trojanowski, J.Q., Shaw, L.M., Jack Jr., C.R., Petersen, R.C., Aisen, P.S., Jagust, W.J., Koeppe, R.A., Mathis, C.A., Weiner, M.W., Thompson, P.M., 2010. 3D PIB and CSF biomarker associations with hippocampal atrophy in ADNI subjects. Neurobiol. Aging 31 (8), 1284–1303 (PubMed PMID: 20538372).

Cicchetti, D.V., Feinstein, A.R., 1990. High agreement but low kappa: II. Resolving the paradoxes. J. Clin. Epidemiol. 43 (6), 551–558.

Cohen, J.A., 1960. A coefficient of agreement for nominal scales. Educ. Psychol. Meas. 20, 37–46.

Cohen, A.D., Mowrey, W., Weissfeld, L.A., Aizenstein, H.J., McDade, E., Mountz, J.M., Nebes, R.D., Saxton, J.A., Snitz, B., Dekosky, S., Williamson, J., Lopez, O.L., Price, J.C., Mathis, C.A., Klunk, W.E., 2013. Classification of amyloid-positivity in controls: comparison of visual read and quantitative approaches. Neuroimage. 71, 207–215. http://dx.doi.org/10.1016/j.neuroimage.2013.01.015 (Epub 2013/01/29, PubMed PMID: 23353602, PubMed Central PMCID: PMC3605888).

Curtis, C., Gamez, J.E., Singh, U., Sadowsky, C.H., Villena, T., Sabbagh, M.N., Beach, T.G., Duara, R., Fleisher, A.S., Frey, K.A., Walker, Z., Hunjan, A., Holmes, C., Escovar, Y.M., Vera, C.X., Agronin, M.E., Ross, J., Bozoki, A., Akinola, M., Shi, J., Vandenberghe, R., Lkonomovic, M.D., Sherwin, P.F., Grachev, I.D., Farrar, G., Smith, A.P.L., Buckley, C.J., McLain, R., Salloway, S., 2015. Phase 3 trial of flutemetamol labeled with radioactive fluorine 18 imaging and neuritic plaque density. JAMA Neurol. 72 (3), 287–294. http://dx.doi.org/10.1001/jamaneurol.2014.4144 (PubMed PMID: WOS:000352157200008).

Engler, H., Klunk, W., Nordberg, A., Blomqvist, G., Holt, D., Wang, Y.M., Bergstrom, M., Huang, G.F., Estrada, S., Debnath, M., Barletta, J., Sandell, J., Wall, A., Antoni, G., Mathis, C., Langstrom, B., 2004. First PET study with a benzothiazol amyloidimaging agent (PIB) in Alzheimer's disease patients and healthy volunteers. Living Brain Alzheimers Dis. 123–137 (PubMed PMID: BIOSIS:PREV200510330819).

Engler, H., Forsberg, A., Almkvist, O., Blomquist, G., Larsson, E., Savitcheva, I., Wall, A., Ringheim, A., Langstrom, B., Nordberg, A., 2006. Two-year follow-up of amyloid deposition in patients with Alzheimer's disease. Brain 129, 2856–2866 (PubMed PMID: ISI:000241783800007).

Fleiss, J.L., 1971. Measuring nominal scale agreement among many raters. Psychol. Bull. 76 (5), 378–382. http://dx.doi.org/10.1037/h0031619 (PubMed PMID: WOS:A1971K852700006).

Furst, A.J., Rabinovici, G.D., Rostomian, A.H., Steed, T., Alkalay, A., Racine, C., Miller, B.L., Jagust, W.J., 2010. Cognition, glucose metabolism and amyloid burden in Alzheimer's disease. Neurobiol. Aging 33 (2), 215–225 (PubMed PMID: 20417582).

Head, S.J., Mokhles, M.M., Osnabrugge, R.L., Pibarot, P., Mack, M.J., Takkenberg, J.J., Bogers, A.J., Kappetein, A.P., 2012. The impact of prosthesis-patient mismatch on long-term survival after aortic valve replacement: a systematic review and meta-analysis of 34 observational studies comprising 27,186 patients with 133,141 patient-years. Eur. Heart J. http://dx.doi.org/10.1093/eurheartj/ehs003 (Epub 2012/03/13, PubMed PMID: 22408037).

Hyman, B.T., Trojanowski, J.Q., 1997. Editorial on consensus recommendations for the postmortem diagnosis of Alzheimer disease from the National Institute on Aging and the Reagan Institute working group on diagnostic criteria for the neuropathological assessment of Alzheimer disease. J. Neuropathol. Exp. Neurol. 56 (10), 1095–1097 (PubMed PMID: WOS:A1997XZ76300002).

Jack, C.R., Bernstein, M.A., Fox, N.C., Thompson, P., Alexander, G., Harvey, D., Borowski, B., Britson, P.J., Whitwell, J.L., Ward, C., Dale, A.M., Felmlee, J.P., Gunter, J.L., Hill, D.L.G., Killiany, R., Schuff, N., Fox-Bosetti, S., Lin, C., Studholme, C., DeCarli, C.S., Krueger, G., Ward, H.A., Metzger, G.J., Scott, K.T., Mallozzi, R., Blezek, D., Levy, J., Debbins, J.P., Fleisher, A.S., Albert, M., Green, R., Bartzokis, G., Glover, G., Mugler, J., Weiner, M.W., 2008. The Alzheimer's Disease Neuroimaging Initiative (ADNI): MRI methods. J. Magn. Reson. Imaging 27 (4), 685–691 (PubMed PMID: WOS:000254709500001).

Kemppainen, N.M., Aalto, S., Wilson, I.A., Nagren, K., Helin, S., Bruck, A., Oikonen, V., Kailajarvi, M., Scheinin, M., Viitanen, M., Parkkola, R., Rinne, J.O., 2007. PET amyloid ligand [C-11]PIB uptake is increased in mild cognitive impairment. Neurology 68 (19), 1603–1606 (PubMed PMID: ISI:000246274600010).

Klunk, W.E., Engler, H., Nordberg, A., Wang, Y., Blomqvist, G., Holt, D.P., Bergström, M., Savitcheva, I., Huang, G.F., Estrada, S., Ausén, B., Debnath, M.L., Barletta, J., Price, J.C., Sandell, J., Lopresti, B.J., Wall, A., Koivisto, P., Antoni, G., Mathis, C.A., Långström, B., 2004. Imaging brain amyloid in Alzheimer's disease with Pittsburgh Compound-B. Ann. Neurol. 55 (3), 306–319 (PubMed PMID: 14991808).

Mason, N., Klunk, W., Debnath, M., Flatt, N., Huang, G., Shao, L., Mathis, C.A., 2009. Synthesis and evaluation of aromatic: fluorinated F-18 pib analogs as abeta plaque pet imaging agents. J. Labelled Compd. Radiopharm. 52, S90-S (PubMed PMID: WOS:000268724900091).

Mathis, C.A., Wang, Y., Holt, D.P., Huang, G.F., Debnath, M.L., Klunk, W.E., 2003. Synthesis and evaluation of ^{11}C-labeled 6-substituted 2-aryl benzothiazoles as amyloid imaging agents. J. Med. Chem. 46, 2740–2754.

Mirra, S.S., Heyman, A., McKeel, D., Sumi, S.M., Crain, B.J., Brownlee, L.M., Vogel, F.S., Hughes, J.P., Vanbelle, G., Berg, L., 1991. The consortium to establish a registry for Alzheimers-disease (Cerad).2. standardization of the neuropathologic assessment of Alzheimers-disease. Neurology 41 (4), 479–486 (PubMed PMID: WOS:A1991FG37700002).

Mormino, E.C., Kluth, J.T., Madison, C.M., Rabinovici, G.D., Baker, S.L., Miller, B.L., Koeppe, R.A., Mathis, C.A., Weiner, M.W., Jagust, W.J., 2009. Episodic memory loss is related to hippocampal-mediated beta-amyloid deposition in elderly subjects. Brain 132 (Pt 5), 1310–1323 (PubMed PMID: 19042931).

Pike, K.E., Savage, G., Villemagne, V.L., Ng, S., Moss, S.A., Maruff, P., Mathis, C.A., Klunk, W.E., Masters, C.L., Rowe, C.C., 2007a. Beta-amyloid imaging and memory in non-demented individuals: evidence for preclinical Alzheimer's disease. Brain 130, 2837–2844 (PubMed PMID: ISI:000250675200012).

Pike, K.E., Savage, G., Villemagne, V.L., Ng, S., Moss, S.A., Maruff, P., Mathis, C.A., Klunk, W.E., Masters, C.L., Rowe, C.C., 2007b. β-amyloid imaging and memory in non-demented individuals: evidence for preclinical Alzheimer's disease. Brain 130 (Pt 11), 2837–2844 (PubMed PMID: 17928318).

Price, J.C., Ziolko, S.K., Weissfeld, L.A., Klunk, W.E., Lopresti, B.J., Hoge, J.A., Lu, X.L., Bi, W.Z., Meltzer, C.C., Tsopelas, N., DeKosky, S.T., Mathis, C.A., 2005. FDG and PIBPET imaging in Alzheimer's disease and mild cognitive impairment. Neuropsychopharmacology 30, S225-S (PubMed PMID: ISI:000233442100583).

Rentz, D.M., Locascio, J.J., Becker, J.A., Moran, E.K., Eng, E., Buckner, R.L., Sperling, R.A., Johnson, K.A., 2010. Cognition, reserve, and amyloid deposition in normal aging. Ann. Neurol. 67 (3), 353–364 (PubMed PMID: 20373347).

Resnick, S.M., Sojkova, J., Zhou, Y., An, Y., Ye, W., Holt, D.P., Dannals, R.F., Mathis, C.A., Klunk, W.E., Ferrucci, L., Kraut, M.A., Wong, D.F., 2010. Longitudinal cognitive decline is associated with fibrillar amyloid-beta measured by [11C]PiB. Neurology 74 (10), 807–815 (PubMed PMID: 20147655).

Rosario, B.L., Weissfeld, L.A., Laymon, C.M., Mathis, C.A., Klunk, W.E., Berginc, M.D., James, J.A., Hoge, J.A., Price, J.C., 2011. Inter-rater reliability of manual and automated region-of-interest delineation for PiB PET. Neuroimage 55 (3), 933–941 (PubMed PMID: ISI:000288313800009).

Rowe, C.C., Ng, S., Ackermann, U., Gong, S.J., Pike, K., Savage, G., Cowie, T.F., Dickinson, K.L., Maruff, P., Darby, D., Smith, C., Woodward, M., Merory, J., Tochon-Danguy, H., O'Keefe, G., Klunk, W.E., Mathis, C.A., Price, J.C., Masters, C.L., Villemagne, V.L., 2007. Imaging beta-amyloid burden in aging and dementia. Neurology 68 (20), 1718–1725 (PubMed PMID: ISI:000246450500012).

Spitzer, R.L., Fleiss, J.L., 1974. A re-analysis of the reliability of psychiatric diagnosis. Br. J. Psychiatry 125, 341–372.

Vandenberghe, R., Van Laere, K., Ivanoiu, A., Salmon, E., Bastin, C., Triau, E., Hasselbalch, S., Law, I., Andersen, A., Korner, A., Minthon, L., Garraux, G., Nelissen, N., Bormans, G., Buckley, C., Owenius, R., Thurfjell, L., Farrar, G., Brooks, D.J., 2010. ^{18}F-flutemetamol amyloid imaging in Alzheimer disease and mild cognitive impairment: a phase 2 trial. Ann. Neurol. 68 (3), 319–329. http://dx.doi.org/10.1002/ana.22068 (Epub 2010/08/06, PubMed PMID: 20687209).

Wilson, A.A., Garcia, A., Chestakova, A., Kung, H., Houle, S., 2004. A rapid one-step radiosynthesis of the beta-amyloid imaging radiotracer N-methyl-C-11 2-(4′-methylaminophenyl)-6-hydroxybenzothiazole (C-11-6-OH-BTA-1). J. Labelled Compd. Radiopharm. 47 (10), 679–682. http://dx.doi.org/10.1002/jlcr.854 (PubMed PMID: WOS:000224594000006).

Wolk, D.A., Grachev, I.D., Buckley, C., Kazi, H., Grady, M.S., Trojanowski, J.Q., Hamilton, R.H., Sherwin, P., McLain, R., Arnold, S.E., 2011. Association between in vivo fluorine 18-labeled flutemetamol amyloid positron emission tomography imaging and in vivo cerebral cortical histopathology. Arch. Neurol. 68 (11), 1398–1403. http://dx.doi.org/10.1001/archneurol.2011.153 (PubMed PMID: WOS:000297014900005).

Woods, R.P., Mazziotta, J.C., Cherry, S.R., 1993. MRI–PET registration with automated algorithm. J. Comput. Assist. Tomogr. 17 (4), 536–546 (PubMed PMID: WOS:A1993LM74900004).